The Effect of the Head Size on the Ear-to-Ear Radio-Propagation Channel for Body-Centric Wireless Networks

Kvist, Søren Helstrup; Thaysen, Jesper; Jakobsen, Kaj Bjarne

Published in:
Antennas and Propagation Conference (LAPC)

Link to article, DOI:
10.1109/LAPC.2010.5666270

Publication date:
2010

Document Version
Publisher's PDF, also known as Version of record

The Effect of the Head Size on the Ear-to-Ear Radio-Propagation Channel for Body-Centric Wireless Networks

Søren H. Kvist*†, Jesper Thaysen† and Kaj B. Jakobsen*
shk@elektro.dtu.dk, jthaysen@gnresound.dk, kbj@elektro.dtu.dk

*Department of Electrical Engineering, Electromagnetic Systems, Technical University of Denmark, Ørsteds Plads, Building 348, DK-2800 Kgs. Lyngby, Denmark.

†GN ReSound A/S, Lautrupbjerg 7, DK-2750 Ballerup, Denmark.

***Abstract*—The effect of the head size on the ear-to-ear radio-propagation channel as a part of a body-centric wireless network is examined. The channel quality is evaluated at $2.45\,\mathrm{GHz}$ in terms of path gain ($|S_{21}|$) between two monopole antennas that are placed normal to the surface of the head. The investigation is done by measurements and HFSS simulations. It is found that the characteristics of the head may cause constructive or destructive interference that may result in up to $10\,\mathrm{dB}$ variation in the path gain.**

I. Introduction

The advent of body-worn wireless electronic devices has spurred a large interest in the characterization and analysis of the propagation of electromagnetic waves around the human body, e.g. [1]–[7]. In [1] the ear-to-ear path gain ($|S_{21}|$) is evaluated with UWB antennas (1.5–$8.0\,\mathrm{GHz}$) fixed at the sides of the head. It was found that the electromagnetic field propagates around the head, rather than through it, due to the large tissue losses at these frequencies. Furthermore, it was concluded that diffraction, as opposed to surface waves, is the dominant propagation mechanism around the head. Many other works, such as [2]–[4], conclude rather intuitively that on-body antennas need to radiate tangentially to the surface of the body, with nulls in the directions towards and away from the body. Furthermore, the best path gain is obtained when the antennas are polarized normal to the body. For example, a dipole placed normal to the body will result in a better path gain than an equivalent loop antenna, even though both antennas radiate tangentially to the body surface. In [4], the human head is modeled as a sphere using spherical vector wave expansion. The path gain along the surface of the head is examined as a function of the angle between the point source excitation and the observation point. It is found that excitation by hertzian dipoles that are normal to the surface of the sphere in general provides the best path gain, except for angles close to 180 degrees. Similarly, the human head is modeled as an infinitely long cylinder in [7]. The path gain around the cylinder is evaluated as a function of the distance in cm along its surface. It is found that significant interference occurs between waves that travel around the cylinder in clockwise and counter-clockwise directions. The present work examines the $2.45\,\mathrm{GHz}$ path gain between monopole antennas that are placed orthogonal to the human head. The path gain is considered as a function of the distance around-the-back and over-the-top of the head. The distance is measured in free space wavelengths, λ_0. Compared to previous theoretical studies, the present work is focused on practical measurements that are made by the use of a realistic SAM head phantom. The measurements are compared to results obtained from Ansoft HFSS v.12 [8] simulations.

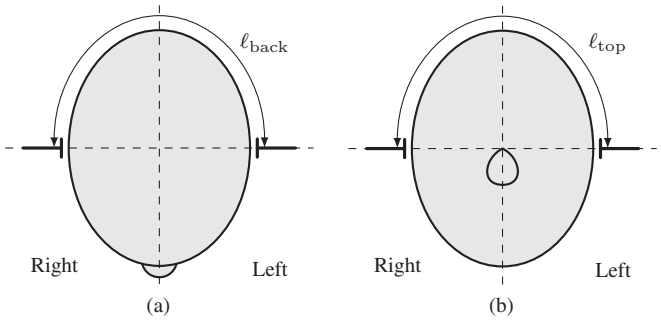

Fig. 1. Monopole antennas are mounted normal to the surface of the head and moved towards the back (a) and top (b) of the head in two series of measurements and simulations.

II. Setup

The experimental setup is depicted in Fig. 1. The path gain is evaluated in two series of measurements and simulations. First, the antennas on both sides of the head are simultaneously moved towards the back of the head in equally sized steps. The monopoles are kept normal to the surface of the head at all times. S-parameters are obtained at each step, and the distance between the antennas around the back of the head, as shown in Fig. 1a, is logged. In the second series, the antennas are moved towards the top of the head in a similar manner. The S-parameters are now logged along with the distance between the antennas over the top of the head, as indicated in Fig. 1b. A standard SAM head phantom was used in the measurements, as seen in Fig. 2a. The monopole antennas are $1\,\mathrm{mm}$ in diameter and have lengths $0.29\lambda_0$. They

978-1-4244-7307-6/10/$26.00 ©2010 IEEE

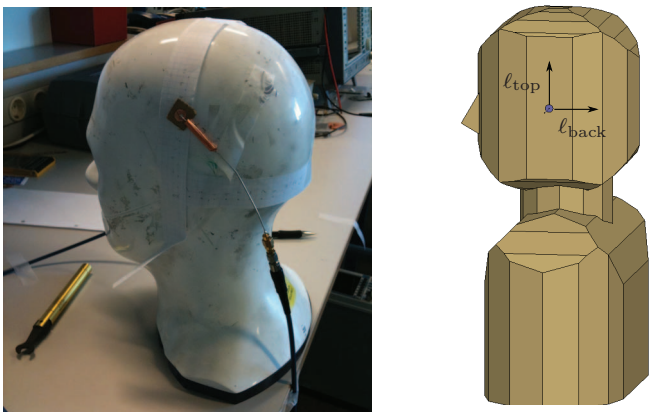

(a) (b)

Fig. 2. A standard SAM head phantom was used in the measurements (a). The monopole antenna cables were mounted with sleeve baluns, in order to reduce the radiation from the cables. A numerical phantom was used for the HFSS simulations (b).

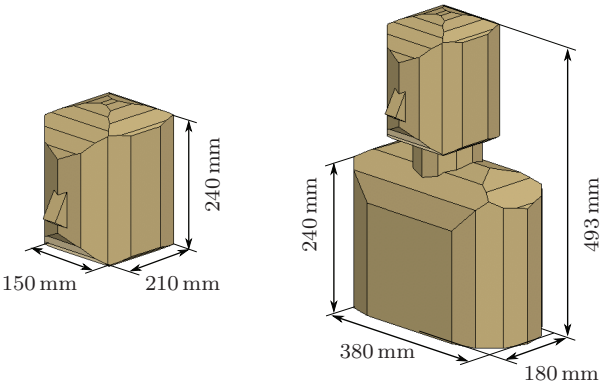

(a) (b)

Fig. 3. Coarse homogeneous models of the human head (a) and the human head and torso (b). The models are constructed for use with Ansoft HFSS [5]. The material parameters are relative permittivity $\epsilon_{\text{r}} = 39.2$ and conductivity $\sigma = 1.80\,\text{S/m}$ [10].

are mounted on small circular ground planes with $10\,\text{mm}$ diameters. The monopoles were held in place with ordinary household tape, during each measurement. The coaxial cables feeding the monopoles were mounted with sleeve baluns in order to prevent the feed cables from radiating. A vector network analyzer performed a running average of 64 samples at 201 frequency points in the range 2–3 GHz in order to get stable S-parameter measurements. Evaluation of the measured path gain indicated that some reflections occurred during the measurements. This was especially visible as ripples in $|S_{21}|$ when the antennas were mounted on opposite sides of the head and the signal diffracted around the head was weak. Further inspection of the time domain signal revealed that delayed parts of the response were almost identical when comparing measurements where the antennas were differently spaced. These delayed parts of the response were identified as

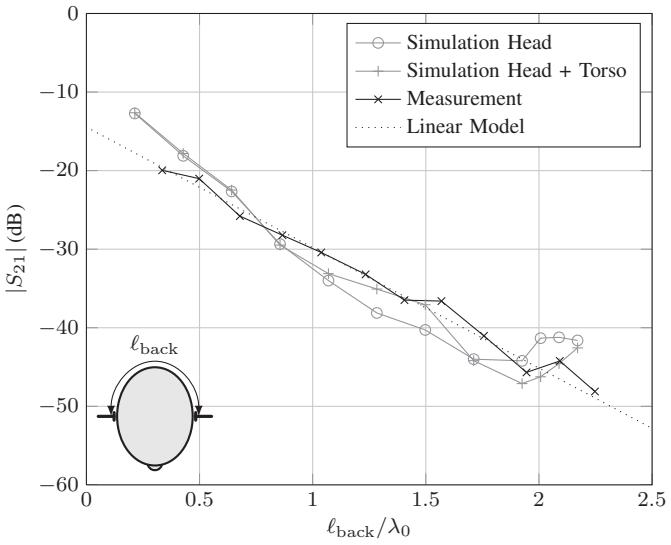

Fig. 4. Measured and simulated path gain ($|S_{21}|$) at 2.45 GHz versus relative distance around the back of the head, $\ell_{\text{back}}/\lambda_0$ for $\ell_{\text{top}} \approx 2.9\lambda_0$.

reflections, which were subsequently removed by time-gating as in [9], except a hamming window was applied instead of a rectangular one. The time-gating removed the ripples that were observed in the frequency domain. The measurements were validated by Ansoft HFSS v.12 [8] simulations. Coarse homogeneous models of the human head and torso were implemented in software [5]. The models are seen in Fig. 3. The material parameters are relative permittivity $\epsilon_{\text{r}} = 39.2$ and conductivity $\sigma = 1.80\,\text{S/m}$ [10]. The simulated monopole antennas had the same physical dimensions as the monopoles that were used in the measurements. The feed was lumped ports placed between the monopole itself and the tiny ground plane. Hence, no feed cables were included in the simulations.

III. Results and Discussion

The path gain measurements and the corresponding simulation results are displayed in Fig. 4 and Fig. 5, for the measurement and simulation series around the back and top of the head, respectively. In the case where the antennas are moved towards the back of the head, the path gain exhibits an almost linear dependence on the distance around the back, ℓ_{back}, on the logarithmic scale in Fig. 4. This is highlighted by a fitted linear model that is shown as a dotted line in the figure. This behavior is expected, since equivalent results have previously been reported for propagation around the body, e.g., in [2], [6]. For distances where $\ell_{\text{neck}} \geq 1.9\lambda_0$ the distances around the front and the back of the head are comparable. In this region the measurements and both simulations display a deviation from the linear model. This is due to interference between waves that travel around the front, back and top of the head. Very similar results were reported in [7]. An excellent overall agreement is observed between the measured and the simulated path gain. When the distance around the back is kept constant at $\ell_{\text{back}} \approx 2.25\lambda_0$, and the antennas are moved towards the top of the head, an interesting phenomenon occurs,

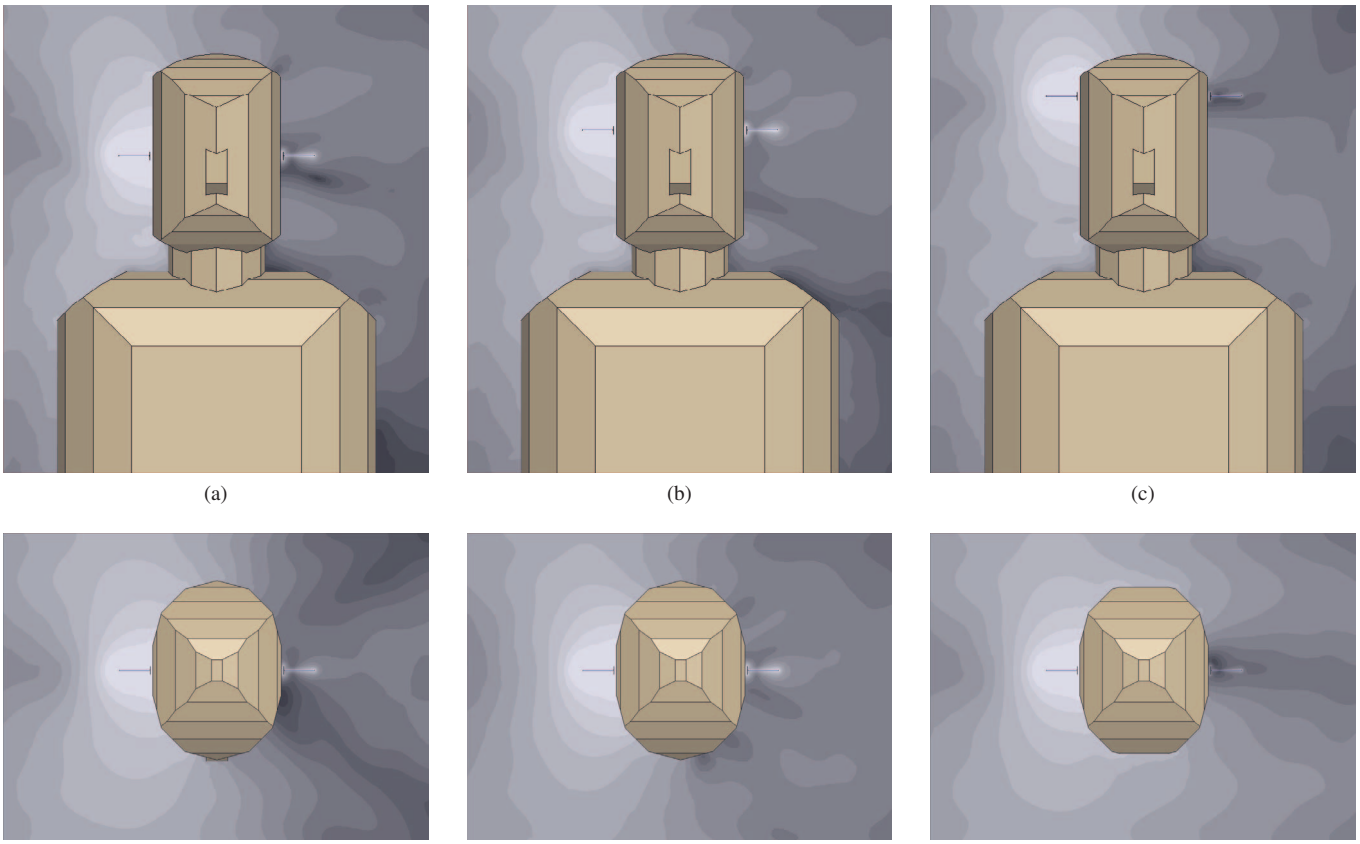

Fig. 6. Simulated magnitude of the electric field that is radiated by the monopole at the right ear. The electric field is shown for $\ell_{\text{top}} \approx 2.75\lambda_0$ and $\ell_{\text{back}} \approx 2.25\lambda_0$ (a), (d), $\ell_{\text{top}} \approx \ell_{\text{back}} \approx 2.25\lambda_0$ (b), (e) and $\ell_{\text{top}} \approx 1.75\lambda_0$ and $\ell_{\text{back}} \approx 2.25\lambda_0$ (c), (f). The logarithmic color scale ranges from $1\,\text{V/m}$ (black) to $25\,\text{V/m}$ (white). The plots (a), (b) and (c) show the front view, while (d), (e) and (f) show the top view in the horizontal plane of the monopoles.

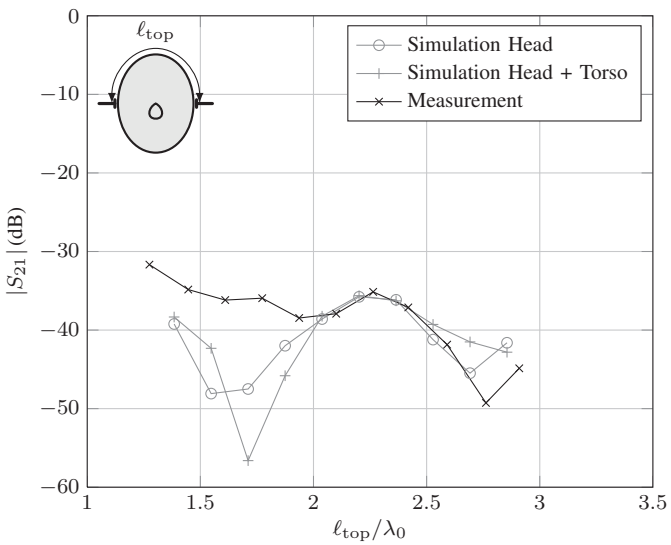

Fig. 5. Measured and simulated path gain ($|S_{21}|$) at 2.45 GHz versus relative distance over the top of the head, $\ell_{\text{top}}/\lambda_0$ for $\ell_{\text{back}} \approx 2.25\lambda_0$.

as seen on Fig. 5. The path gain seems to vary by more than 10 dB as a function of ℓ_{top}, with maxima and minima separated by $\lambda_0/2$. It is noticeable that the local maximum in the path gain appears at $\ell_{\text{top}} \approx 2.25\lambda_0$, which coincides with the distance around the back of the head, ℓ_{back}. This suggests that the signal that is received at the other ear is the sum of two dominant signals, one around the back and one over the top, that are added in phase. Similarly, at the local minima it is clear that these two signals are added out of phase, such that $\ell_{\text{top}} = \ell_{\text{back}} \pm \lambda_0/2$. The values of the path gain at the two minima and at the maximum are collected in Table I for comparison. In this second series of measurements and simulations, there is an excellent agreement between both simulations and measurements when the antennas are separated by a large distance over the top of the head, $\ell_{\text{top}}/\lambda_0 > 2$. However, when the antennas are close to the

TABLE I
COMPARISON OF THE MEASURED AND SIMULATED PATH GAINS ($|S_{21}|$) AT THE TWO MINIMA, WHERE ℓ_{top} AND ℓ_{back} DIFFER BY $\lambda_0/2$ AND THE MAXIMUM WHERE $\ell_{\text{top}} = \ell_{\text{back}}$.

$\ell_{\text{top}} - \ell_{\text{back}}$	(λ_0)	-0.5	0.0	0.5
Sim. Head	(dB)	-46	-36	-44
Sim. Head + Torso	(dB)	-56	-36	-42
Measurement	(dB)	-37	-35	-48

top of the head, $\ell_{\mathrm{top}}/\lambda_0 < 2$, there is a significant deviation. The local minimum in path gain at $\ell_{\mathrm{top}} \approx 1.75\lambda_0$ is only observed in the simulated path gains, and not present in the measurements. This is due to the differences between the more realistic SAM phantom head and the coarse computer models. In the models, ℓ_{back} is truly kept constant for all values of ℓ_{top} due to the geometry of the model heads. Yet, this is not the case for the SAM head (and most likely any real human head) as evident from Fig. 2. As ℓ_{top} is decreased, so is ℓ_{back} in this case, thus avoiding destructive interference. The variation in the path gain is clearly visible in the electric-field distributions that are shown in Fig. 6. The field plots show the complex magnitude of the simulated total electric field at the maximum and minimum of the path gain curve in Fig. 5, for three different values of ℓ_{top}. Only the antenna at the right ear is radiating in these field plots. The logarithmic color scale ranges from $1\,\mathrm{V/m}$ (black) to $25\,\mathrm{V/m}$ (white). Fig. 6a and Fig. 6d show a front view and a top view in the plane of the antennas, respectively, of the case where $\ell_{\mathrm{top}} - \ell_{\mathrm{back}} \approx 0.5\lambda_0$. Destructive interference at the receiving antenna is clearly visible. In comparison, Fig. 6b and Fig. 6e show equivalent views of the electric-field distribution for $\ell_{\mathrm{top}} - \ell_{\mathrm{back}} \approx 0$. In this case is is seen that constructive interference occurs, such that the electric field is stronger at the receiving antenna. Finally, Fig. 6c and Fig. 6f show the electric-field distribution for $\ell_{\mathrm{top}} - \ell_{\mathrm{back}} \approx -0.5\lambda_0$. Destructive interference at the receiving antenna is clearly visible.

IV. Conclusions

The measurements and the simulations agree quite nicely, especially for realistic positions of the antennas, i.e., at the ears. This suggests that the coarse models of the human head is adequate in order to estimate the ear-to-ear path gain through computer simulations, at least for antennas polarized normal to the head. Furthermore, it can be concluded that the ear-to-ear path gain can vary by as much as $10\,\mathrm{dB}$, depending on the features of the specific head. Some heads will show constructive interference with $\ell_{\mathrm{top}} = \ell_{\mathrm{back}} + p\lambda_0$, where $p \in \{0, 1\}$, while others will experience destructive interference as $\ell_{\mathrm{top}} = \ell_{\mathrm{back}} \pm \lambda_0/2$. However, most persons will probably fall somewhere in between, as is the case for the SAM head phantom.

References

[1] T. Zasowski, G. Meyer, F. Althaus, and A. Wittneben, "Uwb signal propagation at the human head," *IEEE Trans. Microw. Theory Tech.*, vol. 54, no. 4, Part 2, pp. 1836–1845, Jun 2006.

[2] P. S. Hall, Y. Hao, Y. Nechayev, A. Alomainy, C. C. Constantinou, C. Parini, M. Kamarudin, T. Salim, D. Hee, R. F. Dubrovka, A. Owadally, W. Song, A. Serra, P. Nepa, M. Gallo, and M. Bozzetti, "Antennas and propagation for on-body communication systems," *IEEE Antennas Propag. Mag.*, vol. 49, no. 3, pp. 41–58, Jun 2007.

[3] A. Khaleghi and I. Balasingham, "Non-line-of-sight on-body ultra wideband (1-6 ghz) channel characterisation using different antenna polarisations," *Microwaves, Antennas & Propagation, IET*, vol. 3, no. 7, pp. 1019–1027, Oct 2009.

[4] B. Nour and O. Breinbjerg, "Electromagnetic power flow between opposite sides of a lossy dielectric sphere using spherical vector wave expansion," *EuCAP 2010*, p. 5, Apr 2010.

[5] S. H. Kvist and K. B. Jakobsen, "Investigation of the chest-ear radio propagation channel," *EuCAP 2010*, p. 3, Apr 2010.

[6] A. Fort, F. Keshmiri, G. Crusats, C. Craeye, and C. Oestges, "A body area propagation model derived from fundamental principles: Analytical analysis and comparison with measurements," *IEEE Trans. Antennas Propag.*, vol. 58, no. 2, pp. 503–514, Feb 2010.

[7] T. Alves, B. Poussot, J.-M. Laheurte, H. Terchoune, M. Wong, and V. F. Hanna, "Analytical propagation modelling of ban channels based on the creeping wave theory," *EuCAP 2010*, pp. 1–5, Apr 2010.

[8] Ansoft, *HFSS v.12 User Guide*, 2008.

[9] R. Zentner, M. Dadic, Z. Sipus, and J. Bartolic, "Time domain analysis of mutual coupling measurements between stacked patches," *Applied Electromagnetics and Communications, 2003. ICECom 2003. 17th International Conference on*, pp. 370–373, 2003.

[10] J. Volakis, *Antenna engineering handbook*. McGraw-Hill Professional, 2007, ch. 36.